Memory effects in avalanche dynamics: a key to the statistical properties of earthquakes

E. A. Jagla

Centro Atómico Bariloche and Instituto Balseiro,
Comisión Nacional de Energía Atómica, (8400) Bariloche, Argentina

François P. Landes and Alberto Rosso

Laboratoire de Physique Théorique et Modèles Statistiques (UMR CNRS 8626), Université Paris-Sud, Orsay, France

Many complex systems respond to continuous input of energy by accumulation of stress over time and sudden energy releases in the form of avalanches. Avalanches are paradigmatic non-equilibrium phenomena displaying power law size distribution and involving all the length scales in the system. Conventional avalanche models disregard memory effects and thus miss basic features observed in real systems. Notable examples are aftershocks and the anomalous exponent of the Gutenberg-Richter law which characterize earthquake statistics. We propose a model which accounts for memory effects through the introduction of viscoelastic relaxation at an intermediate time scale. We demonstrate that in the resulting dynamics, coherent oscillations of the stress field emerge spontaneously without fine tuning of any parameter. Remarkably, in two dimensions, which is relevant in seismicity, these oscillations generate instability patterns that produce realistic earthquake dynamics with the correct Gutenberg-Richter exponent.

The driven dynamics of heterogeneous systems often proceeds by random jumps called avalanches, which display scale-free statistics. This critical out-of-equilibrium behaviour emerges from the competition between internal elastic interactions and heterogeneities, and is understood in the framework of the depinning transition [1, 2]. Remarkably, one can often disregard the precise details of the microscopic dynamics when considering the large scale behavior. As a result, various phenomena such as the Barkhausen noise in ferromagnets [2, 3, 5], the crack propagation in brittle materials [6–8] or the wetting fronts moving on rough substrate [9–11] may display the very same avalanche statistics.

A key feature of this description is the lack of internal time scales characterizing the memory of the system [1, 12]. However, the inclusion of processes relaxing internal constraints introduces memory effects in the dynamics, with their own characteristic time. The existence of this kind of relaxation may have drastic consequences on the macroscopic behaviour of the system, as in the context of friction where it generates the time increase of static friction during the contact between two surfaces at rest [13, 14]. Here we show how these relaxation processes generically induce a novel avalanche dynamics characterized by new critical exponents and bursts of aftershocks strongly correlated in time and space.

We account for the presence of relaxation processes by introducing viscoelastic interactions, which generate a new, emerging time scale. Due to its simplicity, the model allows for analytic treatment in the mean field, and for extensive numerical simulations in finite dimensions. Our main observations are twofold. First, in mean field the new time scale is associated with a dynamical instability, which is responsible for periodic oscillations of the stress in the entire system. This instability, named *avalanche oscillator*, was observed in numerical simula-

tions and experiments of compression of Nickel micro crystals [15]. The viscoelastic interactions are at the root of the *avalanche oscillator*: they drive the system towards a critical point, that we prove to be unstable. Second, in two dimensions the global oscillations found in mean field remain coherent only on small regions. In each region the oscillations of the local stress have roughly the same amplitude and period, but different phases, so that at a given time the stress map displays a terraced structure.

We claim that the relaxation processes studied in our model are essential to capture the basic features of seismic dynamics. In particular, the new time scale is the one involved in the aftershock phenomenon [16–18]. Moreover the oscillations of the stress field explain the quasi-periodic time recurrence of earthquakes that emerges from the data analysis of the seismic activity in some geographical areas [19, 20]. Finally we show that in two dimensions, the exponent of the avalanche size distribution becomes perfectly consistent with that of the actual Gutenberg-Richter law, and the aftershock spatial correlations obtained have strong similarities with the *migration effect* observed in real earthquakes [21].

I. FROM CONVENTIONAL DEPINNING TO THE MODEL WITH RELAXATION

Our model with relaxation is constructed upon the paradigmatic model of avalanche dynamics, describing the depinning of a d-dimensional elastic interface moving inside a $d + 1$ dimensional space [1]. In this model, the interface consists in a collection of blocks (see Fig. 1a) obeying the equation of motion:

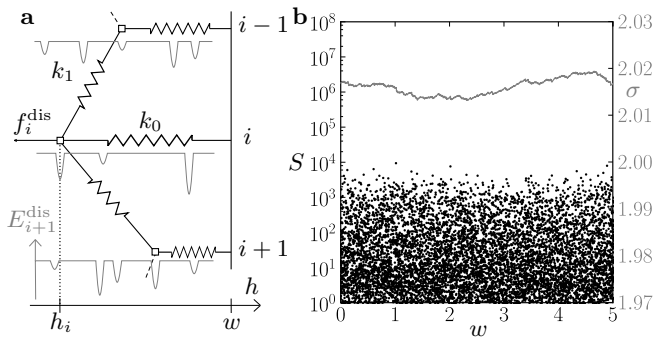$$\eta \partial_t h_i = k_0(w - h_i) + f_i^{\text{dis}}(h_i) + k_1 \Delta h_i \qquad (1)$$

FIG. 1: **Conventional depinning model.** (**a**) Schema of the system for $d = 1$. Only disorder and elastic interactions (with spring constants k_0, k_1) control the dynamics of the blocks, located in h_i, h_{i+1}, etc. The disordered force derives from the pinning potential pictured in grey: $f_i^{\text{dis}} = -\partial E_i^{\text{dis}}(h_i)/\partial h_i$. (**b**) Numerical results showing sequence of avalanches sizes S and the stress σ (grey) as a function of the drive w. The sequence displays a Poissonian behaviour and the small fluctuations of the stress are due to the finite size.

where (i, h_i) is the $d + 1$-dimensional coordinate of the block and η is the viscosity of the medium. Each block feels elastic interactions via the (discrete) Laplacian term $k_1 \Delta h_i$, disorder via $f_i^{\text{dis}}(h_i)$ and is driven towards the position $w = V_0 t$ via springs of elasticity k_0. The force per unit area applied by the drive, namely the stress, is given by:

$$\sigma = k_0(w - \overline{h}), \qquad (2)$$

where $\overline{h}$ is the mean value of interface height. The slow increase of w over time induces an augmentation of the pulling force on each block. As a response, blocks typically adjust slightly their positions, but sometimes a block reaches a mechanical unstable state and moves far away from its position to a new local energy minimum. This can in turn destabilize neighbouring blocks, thus triggering an avalanche event that we characterize by its size S, defined as the volume swept by the interface during the event. In Fig. 1b we show the sizes S of a sequence of avalanches obtained by driving w quasi-statically ($V_0 = 0^+$). The sequence displays a Poissonian behaviour, in the sense that both the sizes and the temporal locations of the events are uncorrelated variables. Moreover the stress is constant in time, with small fluctuations due to finite size effects.

Our modified model consists in replacing the springs k_1 by viscoelastic elements, built using springs and dashpots, as depicted in Fig. 2a. Its dynamical equations are:

$$\eta \partial_t h_i = k_0(w - h_i) + f_i^{\text{dis}}(h_i) + k_1 \Delta h_i + k_2(\Delta h_i - u_i) \qquad (3)$$

$$\eta_u \partial_t u_i = k_2(\Delta h_i - u_i), \qquad (4)$$

where the auxiliary variables u_i depend on the elongation of the neighbouring dashpots: in one dimension this variable reads $u_i = (\phi_i - h_i) + (h_{i-1} - \phi_{i-1})$ (see Appendix A). The relaxation constant η_u sets a new characteristic time $\tau_u = \eta_u/k_0$, to be compared with the two scales of the depinning model: (i) $\tau_D = \overline{z}/V_0$ which accounts for the slow increase of the external drive w (where $\overline{z}$ is the typical microscopic disorder length scale), (ii) $\tau = \eta/k_0$, which is the response time to a perturbation. Note that τ corresponds to the avalanches duration, τ_D is the time between two consecutive main shocks and τ_u sets the scale of aftershocks.

For simplicity of the analysis, we assume here that the three scales are well separated, namely $\tau \ll \tau_u \ll \tau_D$ (i.e. $\eta \ll \eta_u$). In this limit, on the time scale τ the dashpots are completely rigid, so that the u_i's are constant in time and the dynamics is exactly the same as for the depinning model with elastic constant $k_1 + k_2$. However, after an avalanche, and in a time scale τ_u, the h_i's are pinned and the u_i variables relax exponentially:

$$u_i(t) = \Delta h_i + (u_i(t_0) - \Delta h_i)e^{-(t-t_0)k_2/\eta_u}, \quad \forall i, \quad (5)$$

where t_0 is the time at which the last avalanche occurred. The effect of relaxation is to suppress the term $k_2(\Delta h_i - u_i)$ in Eq.(D1), so that some blocks may become unstable. This triggers secondary avalanches in the system, identified with aftershocks in the seismic context. Aftershocks occur without any additional driving: the ensemble of events that occur at a single value of w will be called a *cluster* of events (see Fig. 2b). When $u_i = (\Delta h)_i$ for all i, the system is in the *fully relaxed* state and new instabilities can only be triggered by an increase of w. Note that this state corresponds to a stable configuration of the depinning model with same k_0, same disorder realization and elastic constant k_1.

In Fig. 2 we show the typical behaviour of the model in two dimension (b) and in the mean field approximation (c). We observe that unlike depinning, the dynamics is qualitatively very different in the two cases. In mean field the stress displays periodic global oscillations while in two dimensions similar oscillations are observed only on local scales.

II. THE NARROW WELLS APPROXIMATION

To efficiently study Eqs. (1), (D1), (D2), we adopt the so-called "narrow wells" approximation. In this scheme, the disorder is modelled as a collection of narrow pinning wells representing impurities (see Fig. 1a). Along the h direction, the pinning wells are separated by random intervals z with distribution $g(z)$ and mean length $\overline{z}$. A natural choice for $g(z)$ is the exponential law, which corresponds to the case where impurities are uncorrelated in space. If the spatial extension of the wells is negligible compared to $\overline{z}$, we can safely assume that each block is always located in one of those wells, so that its coordi-
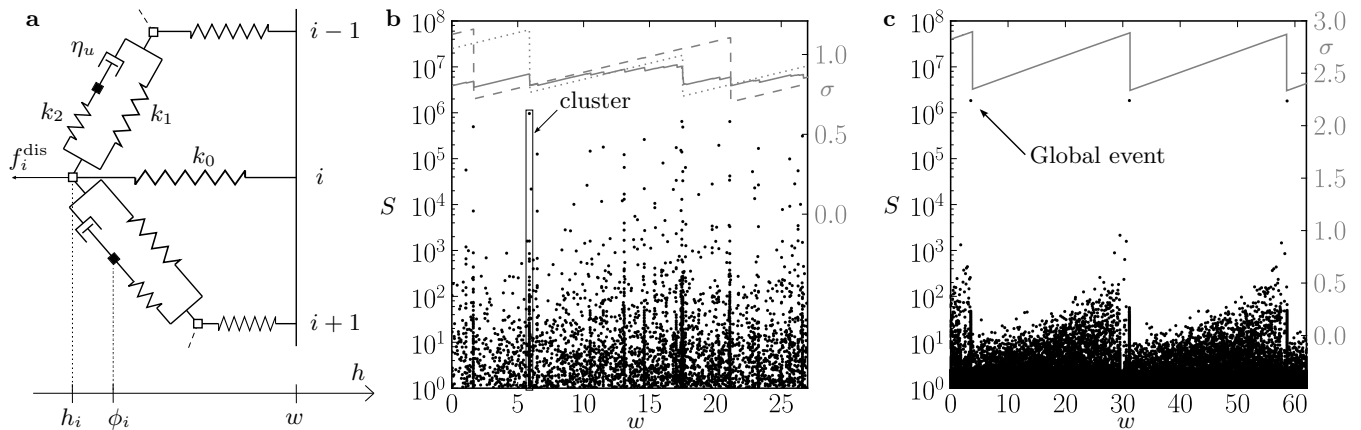
FIG. 2: **Model with relaxation.** (a) Schema of the system for $d = 1$. The introduction of dashpots (with relaxation constant η_u) strongly modifies the elastic interactions between blocks: fast moving blocks feel stiff interactions ($k_1 + k_2$) while pinned block feel softer interactions (k_1). Numerical results showing sequence of avalanches sizes S and stress σ (grey) as a function of the drive w for the $d = 2$ dimensional case (b) and in mean field approximation (c). In two dimensions, we observe aftershocks which corresponds to *clusters* of avalanches that occur at the same value of w. Dashed and dotted grey lines correspond to the local stress of two distant regions: their oscillations have roughly the same period and amplitude, but are not synchronized. In mean field approximation, the dynamics acquires a global periodic time dependence. The steady stress increase culminates in a system size avalanche (*global event*) that abruptly reduces stress by a finite amount.

nate h_i evolves only by discrete jumps z. To exit from a well, a block needs to be pulled by a force larger than a threshold f_i^{th} related to the well's depth.

Within this approximation, the continuous dynamics of the blocks can be re-written as a set of simple rules for the variable δ_i which measures the remaining stability range of the block i. In the depinning model δ_i reads:

$$\delta_i \equiv f_i^{\text{th}} - k_0(w - h_i) - k_1 \Delta h_i. \tag{6}$$

If $\delta_i > 0$ for all i, all blocks are stable and pinned in their narrow wells. Increasing the load w, all δ_i's decrease, until a block becomes unstable ($\delta_i = 0$) and moves to the next pinning well ($h_i \mapsto h_i + z$), characterized by a new random threshold f_i^{th}. The unstable block can be the seed of an avalanche because its motion produces a drop $k_1 z$ in the variables δ of the neighbouring blocks. The avalanche event is exhausted when all blocks are stable.

In the model with relaxation, the stability condition reads:

$$\delta_i = f_i^{\text{th}} - k_0(w - h_i) - k_1 \Delta h_i - k_2(\Delta h_i - u_i) > 0. \tag{7}$$

When a site becomes unstable, the dynamics proceeds with the same rules as before, with u_i's kept constant during the avalanche. When the avalanche event is exhausted, a slow relaxation of u_i takes place (Eq. (D2)). This evolution can decrease δ_i's and thus trigger aftershocks.

III. MEAN FIELD ANALYSIS

We analyse the mean field approximation through the fully connected version of the model, which corresponds to replacing Δh_i with $\overline{h} - h_i$ in Eqs. (6) or (7). In this case, all sites are equivalent and the δ_i's are independent and identically distributed variables, characterized by their probability distribution $P_w(\delta)$ which in general depends on the initial condition $P_0(\delta)$ and on the value of w. In the Appendix B, we compute the evolution equations of $P_w(\delta)$ under an infinitesimal increase in w for both models, for $f_i^{\text{th}} = \text{const}$.

For the conventional depinning model, we show that this evolution has a fixed point reached within a finite increase in w, at which $P_w(\delta)$ is given by the function:

$$Q(\delta, k_1) = \frac{1 - G(\frac{\delta}{k_0 + k_1})}{\overline{z}(k_0 + k_1)}, \tag{8}$$

where $G(z) \equiv \int_0^z dz' g(z')$. This indicates that the large time dynamics is stationary, and that the applied stress in the system is constant in time:

$$\sigma(k_1) \equiv f^{\text{th}} - \overline{\delta}(k_1). \tag{9}$$

Further analysis shows that as long as $P_w(0) < (\overline{z}k_1)^{-1}$ the system displays avalanches bounded by a system-size independent cutoff: $S_{\max} = (1 - P_w(0)\overline{z}k_1)^{-2}$. For example, at the fixed point (B4) we have $P_w(0) = Q(0, k_1) = 1/\overline{z}(k_0 + k_1)$, so that $S_{\max} = (\frac{k_0 + k_1}{k_0})^2$. However if $P_w(0) \geq (\overline{z}k_1)^{-1}$ the system becomes unstable and we observe a *global event* involving a finite fraction of the system.
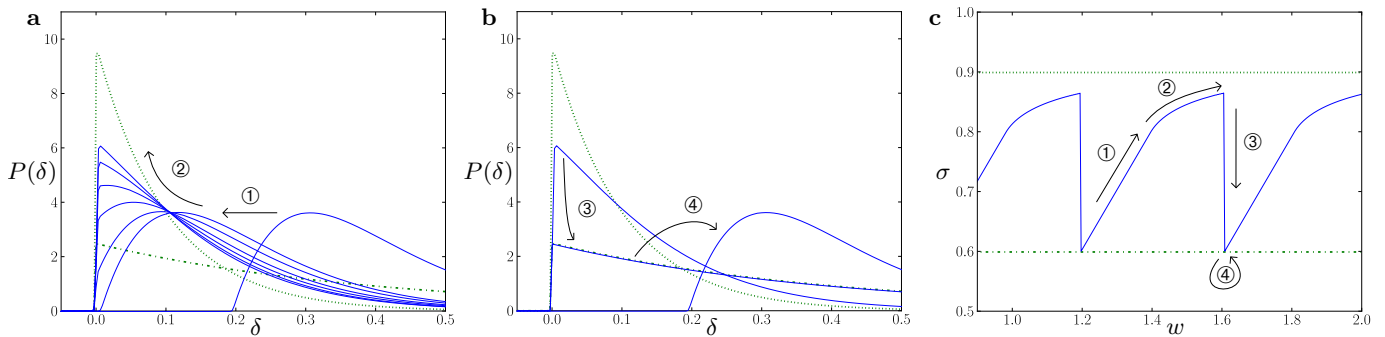
FIG. 3: **Model with relaxation: Mean Field approximation and the avalanche oscillator.** Results of a direct integration of the evolution equations of $P(\delta)$ (see Appendix C). The evolution of the distribution $P(\delta)$ (solid line) and the stress $\sigma = f^{\mathrm{th}} - \overline{\delta}$ (right panel) shows a clear avalanche oscillator dynamics. Four stages during the periodic cycle can be distinguished. Stage 1: driving of the interface, without any avalanche. The stress increases linearly with w. Stage 2: driving with some small events. The stress increases more slowly. The distribution $P(\delta)$ is continuously driven towards the unstable point $Q(\delta, k_1)$ (upper dotted curve) and the stress tends to the value $\sigma(k_1)$ (upper dotted line). Stage 3: a global event is triggered, where $P(\delta)$ reaches the depinning fixed point $Q(\delta, k_1 + k_2)$ (lower dashed curve) and the stress drops to $\sigma(k_1 + k_2)$ (lower dashed line). Stage 4: Relaxation closes the cycle by bringing $P(\delta)$ back to its initial shape, without changing the average stress.

For the model with relaxation, the evolution of $P_w(\delta)$ is non stationary and displays an oscillatory behaviour. Under a small increase in w, two dynamical regimes are observed. On the short time scales ($t \simeq \tau$) sites that become unstable move following the rules of a rigid depinning interface with stiffness $k_1 + k_2$. On longer time scales ($t \simeq \tau_u$), during relaxation, the interface becomes more flexible (with stiffness k_1), thus evolving towards the fixed point $Q(\delta, k_1)$. However when $P_w(0)$ becomes larger than $1/\overline{z}(k_1 + k_2)$, the rigid interface is unstable, so that a single global avalanche drives $P_w(\delta)$ to the rigid fixed point $Q(\delta, k_1 + k_2)$. Finally, this state is deeply altered by relaxation and a new cycle starts. This scenario is confirmed by the numerical integration of the evolution equations (see Appendix C), as shown in Fig 3.

It is interesting that the cyclic behaviour is independent of details of the mean field model. For example the results in Fig. 2c correspond to a case in which the thresholds f_i^{th} are randomly distributed. The avalanche dynamics looks different and displays aftershocks, however the stress is cyclic and global events are also present.

IV. TWO DIMENSIONAL RESULTS AND SEISMIC PHENOMENA

For the two dimensional case we must rely on the results of the numerical implementation of Eqs. (7) and (5) via an efficient method originally developed in [7]. Details are provided in the Appendix D.

The results of a typical run in two dimensions are shown in Fig. 2B. We see a clear distribution of events in clusters of main shocks and aftershocks, as in actual seismicity (where, indeed, any single cluster spans a finite w interval, due to the non-complete separation of time scales). We note that the periodic behaviour observed in
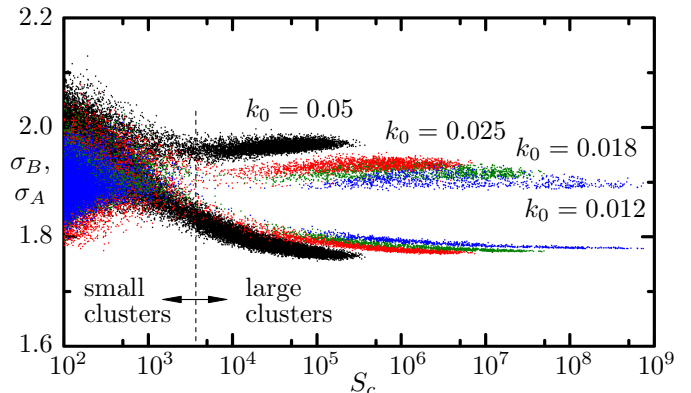

FIG. 4: **Model with relaxation in 2D: emergence of oscillations.** The local stress restricted to the cluster area, just before (up, σ_B) and just after (bottom, σ_A) it takes place, as a function of the cluster size S_C. The vertical dotted line separates the region of "small" and "large" clusters. For sufficiently small values of k_0, it is observed that large clusters move pieces of the interface with stress $\sigma_{\max}$ to a new position with stress $\sigma_{\min}$. A finite difference between $\sigma_{\max}$ and $\sigma_{\min}$ persists even in the limit $k_0 \to 0$.

mean field (Fig. 2C) has disappeared.

Nevertheless, a careful analysis of the two dimensional model shows an interesting reminiscence of the mean field behaviour. In Fig. 4 we compute for each cluster the local stress restricted to the cluster area, just before (σ_B) and just after (σ_A) it takes place (the same analysis performed by studying the events instead of the clusters yields the same results). We see that small clusters show broad distributions of σ_B and σ_A, similar to what would be observed for the depinning case. However for large clusters the two distributions become very narrow: σ_B sets to a value that we denote $\sigma_{\max}$, and σ_A
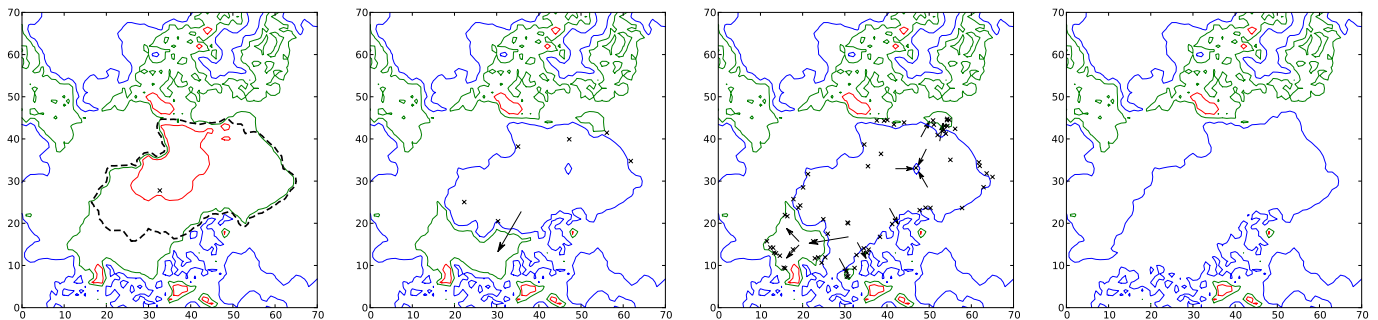
FIG. 5: **Stress map and aftershock sequence.** The contour line plot of the local stress shows a terraced structure. Blue lines correspond to a level $\sim \sigma_{\min}$, red lines to a level $\sim \sigma_{\max}$ and green lines to an intermediate local stress. The epicentre of each large aftershock ($S > 5000$) is indicated by a small cross. First panel from the left: the local stress just before a large event. The dashed line highlights the unstable region (main shock). Second and Third panel: the main shock has stabilized the unstable region which now spreads in the neighbourhood, via the aftershocks (small crosses). The principal directions of expansion of the aftershocks are indicated by black arrows. Last panel: final state after all the aftershocks, when the system is fully relaxed. The total system size is 15000×15000: for each elementary surface of one unit square, the local stress was computed by averaging over a square of 100×100 elemental sites of the discrete system.

sets to $\sigma_{\min}$. This is the fingerprint of the mean field behaviour, and it suggests a large scale description of the two dimensional interface as a terraced structure. Indeed, in Fig. 5, we observe that different parts of the system have different values of the stress, which range from $\sigma_{\min}$ to $\sigma_{\max}$. In analogy with mean field, when the stress of a region reaches a value $\sim \sigma_{\max}$, it gets destabilized and the whole region collapses to $\sigma_{\min}$. In fact the evolution of the local stress associated to a small patch of the interface is non stationary, and shows an almost periodic oscillation between $\sigma_{\min}$ and $\sigma_{\max}$ (Fig. 2B, dashed and dotted lines). However this oscillation is not synchronized among different patches, so that the system does not display a global oscillation. It is remarkable that for the model with relaxation, the width of the distribution of the local stress ($\sim \sigma_{\max} - \sigma_{\min}$) remains finite when $k_0 \to 0$; while in the depinning model [23], it vanishes as $k_0^{1-\zeta/2}$ for very small k_0 (ζ is the roughness exponent of the interface which is found to be smaller than 2). Moreover, our model supports the idea that the seismic activity in a given geographical region displays a quasi-periodic history (the so-called seismic cycle). This periodicity was recently studied in the context of micro-crystals deformation [15], where this oscillatory behavior is named "avalanche oscillator". Similar kind of oscillations were also observed in models with relaxation [23] and in the context of granular materials [24].

A second important feature of the two dimensional model is the spatial distribution of aftershocks in a given cluster (see Fig. 5). After a main shock, many aftershocks follow, extending the slip area. The small ones (not indicated) are rather uniformly distributed inside the slip region; while the epicentres of the large ones typically occur at the border, and extend the slip region. This behaviour has been directly observed in the field and is called "aftershock migration" [21].

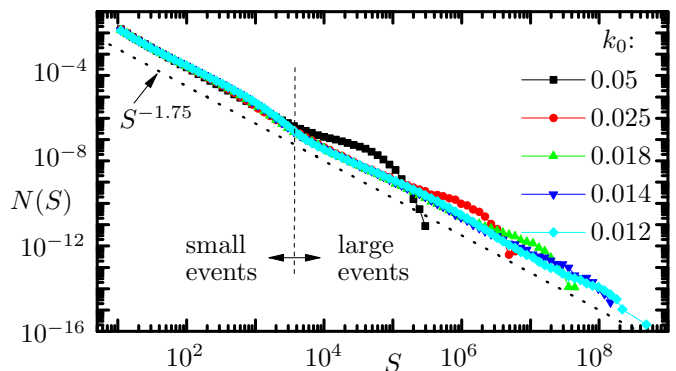As a third point, we discuss the size distribution of the

FIG. 6: **Validation of the Gutenberg-Richter law.** The size distribution of avalanches $N(S)$ is consistent with the exponent $\tau = 1.75$. The dotted line separating the regions of small and large events is indicated: the size distribution does not display any strong feature around this value. The system size is in all cases much larger than the largest avalanche observed, and reaches values of 15000×15000. Other parameters are: $k_1 = 0$, $k_2 = 1$.

avalanches in 2D, presented in Fig. 6. The distribution shows a consistent power law decay in all the range that we have been able to explore (at least in a size range of 10^7) with an *anomalous* exponent $\tau \simeq 1.7 - 1.8$. This is quite remarkable, given that in all conventional avalanche models like depinning or directed percolation, this exponent is always smaller than 1.5, which corresponds to the mean field limit [4, 5]. In particular in the 2D depinning case one measures $\tau \simeq 1.27$. More importantly our result is in very good agreement with the empirical Gutenberg-Richter (GR) law for earthquakes for which $\tau \simeq 1.7$ (Note that historically the magnitude of an earthquake is defined as $M = (2/3)\log_{10} S$. The GR law predicts that $N(M) \sim 10^{-bM}$, with $b \simeq 1$, so that from the definition $N(S) \sim S^{-\tau}$, we have $\tau = 1+2b/3 \simeq 1.7$). A justification

for the value of the GR exponent has been given recently using a forest fire model analogy [27]. It is worth mentioning that this explanation assumes a structure of the interface that is compatible with the one we find here.

V. CONCLUSIONS

Internal relaxation plays crucial roles in the dynamics of sliding objects, and becomes particularly relevant in the large scale realization corresponding to seismic phenomena. It generically induces a tendency for the dynamics to become non-stationary. This tendency fully develops in mean field, where we identify a dynamical instability from which stress oscillations originate. In the most relevant two dimensional case, we provide numerical evidence that the periodic oscillations occur locally, without global synchronization between the different parts of the system. We obtain a size distribution of events compatible with the Gutenberg-Richter law and aftershocks which are spatially distributed similarly to real ones. Furthermore, the viscoelastic elements produce an effective velocity-*weakening* friction law in the system[28], a hallmark of fault dynamics behavior [17], compatible with

the rate-and-state equations, widely used in the macroscopic description of friction [29–31].

Our work reveals that earthquake statistics can be rationalized in terms of collective, *non-stationary* avalanche dynamics. An interesting development of our study would be to characterize the temporally clustered structure of the avalanches. In the viscoelastic model depicted in Fig. 2A, the relaxation is local and controlled by a single time constant. This choice allows a fast computation, but yields an unrealistic exponential decay of the aftershocks over time. In this respect, it would be suitable to consider non-local relaxation mechanisms, as the Laplacian relaxation studied in [28, 32], which can reproduce the observed Omori law.

[1] Fisher, D. S. Collective transport in random media: from superconductors to earthquakes. *Physics Reports* **301**, 113–150 (1998).

[2] Kardar, M. Nonequilibrium dynamics of interfaces and lines. *Physics Reports* **301**, 85–112 (1998).

[3] Alessandro, B., Beatrice, C., Bertotti, G. & Montorsi, A. Domain-wall dynamics and Barkhausen effect in metallic ferromagnetic materials. I. Theory. *Journal of Applied Physics* **68**, 2901–2907 (1990).

[4] Zapperi, S., Cizeau, P., Durin, G. & Stanley, H. Dynamics of a ferromagnetic domain wall: Avalanches, depinning transition, and the Barkhausen effect. *Physical Review B* **58**, 6353–6366 (1998).

[5] Durin, G. & Zapperi, S. The role of stationarity in magnetic crackling noise. *Journal of Statistical Mechanics: Theory and Experiment* **2006**, P01002–P01002 (2006).

[6] Alava, M. J., Nukala, P. K. V. V. & Zapperi, S. Statistical models of fracture. *Advances in Physics* **55**, 349–476 (2006). 0609650.

[7] Bonamy, D., Santucci, S. & Ponson, L. Crackling Dynamics in Material Failure as the Signature of a Self-Organized Dynamic Phase Transition. *Physical Review Letters* **101**, 045501 (2008).

[8] Bonamy, D. & Bouchaud, E. Failure of heterogeneous materials: A dynamic phase transition? *Physics Reports* **498**, 1–44 (2011).

[9] Rosso, A. & Krauth, W. Roughness at the depinning threshold for a long-range elastic string. *Physical Review E* **65**, 025101 (2002).

[10] Moulinet, S., Rosso, A., Krauth, W. & Rolley, E. Width distribution of contact lines on a disordered substrate. *Physical Review E* **69**, 035103 (2004).

[11] Le Doussal, P., Wiese, K. J., Moulinet, S. & Rolley, E. Height fluctuations of a contact line: A direct measurement of the renormalized disorder correlator. *EPL (Europhysics Letters)* **87**, 56001 (2009).

[12] Sethna, J. P., Dahmen, K. A. & Myers, C. R. Crackling noise. *Nature* **410**, 242–50 (2001).

[13] Dieterich, J. H. Time-dependent friction in rocks. *Journal of Geophysical Research* **77**, 3690–3697 (1972).

[14] Marone, C. The effect of loading rate on static friction and the rate of fault healing during the earthquake cycle. *Nature* **391**, 69–71 (1998).

[15] Papanikolaou, S. *et al.* Quasi-periodic events in crystal plasticity and the self-organized avalanche oscillator. *Nature* **490**, 517–21 (2012).

[16] Dieterich, J. H. Time-dependent friction and the mechanics of stick-slip. *Pure and Applied Geophysics PAGEOPH* **116**, 790–806 (1978).

[17] Scholz, C. H. *The Mechanics of Earthquakes and Faulting* (Cambridge Univ Press, 2002).

[18] Ben-Zion, Y. Collective behavior of earthquakes and faults: Continuum-discrete transitions, progressive evolutionary changes, and different dynamic regimes. *Reviews of Geophysics* **46**, RG4006 (2008).

[19] Barbot, S., Lapusta, N. & Avouac, J.-P. Under the hood of the earthquake machine: toward predictive modeling of the seismic cycle. *Science (New York, N.Y.)* **336**, 707–10 (2012).

[20] Ben-Zion, Y. Large earthquake cycles and intermittent criticality on heterogeneous faults due to evolving stress and seismicity. *Journal of Geophysical Research* **108**, 2307 (2003).

[21] Peng, Z. & Zhao, P. Migration of early aftershocks following the 2004 Parkfield earthquake. *Nature Geoscience* **2**, 877–881 (2009).

[22] Grassberger, P. Efficient large-scale simulations of a uniformly driven system. *Physical Review E* **49**, 2436–2444 (1994).

[23] Aragón, L. E., Jagla, E. A. & Rosso, A. Seismic cycles, size of the largest events, and the avalanche size distribution in a model of seismicity. *Physical Review E* **85**, 046112 (2012).

[24] Dahmen, K. a., Ben-Zion, Y. & Uhl, J. T. A simple analytic theory for the statistics of avalanches in sheared granular materials. *Nature Physics* **7**, 554–557 (2011).

[25] Le Doussal, P. & Wiese, K. Driven particle in a random landscape: Disorder correlator, avalanche distribution, and extreme value statistics of records. *Physical Review E* **79**, 051105 (2009).

[26] Dobrinevski, A., Le Doussal, P. & Wiese, K. J. Nonstationary dynamics of the Alessandro-Beatrice-Bertotti-Montorsi model. *Physical Review E* **85**, 031105 (2012).

[27] Jagla, E. A. A forest-fire analogy to explain the b-value of the Gutenberg-Richter law for earthquakes 7 (2013). 1305.1057.

[28] Jagla, E. A. & Kolton, A. B. A mechanism for spatial and temporal earthquake clustering. *Journal of Geophysical Research* **115**, B05312 (2010).

[29] Gu, J.-C., Rice, J. R., Ruina, A. L. & Tse, S. T. Slip motion and stability of a single degree of freedom elastic system with rate and state dependent friction. *Journal of the Mechanics and Physics of Solids* **32**, 167–196 (1984).

[30] Rice, J. R. & Tse, S. T. Dynamic motion of a single degree of freedom system following a rate and state dependent friction law. *Journal of Geophysical Research* **91**, 521 (1986).

[31] Ohmura, A. & Kawamura, H. Rate- and state-dependent friction law and statistical properties of earthquakes. *Europhysics Letters (EPL)* **77**, 69001 (2007).

[32] Jagla, E. A. Realistic spatial and temporal earthquake distributions in a modified Olami-Feder-Christensen model. *Physical Review E* **81**, 046117 (2010).

Appendix A: Depinning with relaxation: derivation of the equations and dynamical properties

The depinning model with relaxation corresponds to the mechanical circuit sketched in Fig. 2**a** of the main text. We first describe the one-dimensional case. The sample is decomposed in blocks of mass m, labelled i and moving along horizontal rails h_i. The action of the dashpot is to resist the change in $\phi_i - h_i$ via viscous friction, with a resulting force on h_i given by $\eta_u \partial_t(\phi_i - h_i)$. The blocks move in a medium with an effective viscosity η, we will study the overdamped regime $m \partial_t^2 h_i \ll \eta \partial_t h_i$[1]. As each block is described by two degrees of freedom h_i and ϕ_i, its time evolution is governed by two equations. The first equation comes from the force balance on h_i:

$$\eta \partial_t h_i = f_i^{\text{dis}}(h_i) + k_0(w - h_i) + k_1(h_{i+1} - h_i)$$
$$+ k_1(h_{i-1} - h_i) + \eta_u \partial_t(\phi_i - h_i) + k_2(\phi_{i-1} - h_i) \quad \text{[A1]}$$

The second equation derives from the force balance on ϕ_i:

$$0 = k_2(h_{i+1} - \phi_i) + \eta_u \partial_t(h_i - \phi_i) \quad \text{[A2]}$$

where we assumed that the internal degree of freedom ϕ_i has no mass. We inject this second equation in the first, and subtract the force balance on ϕ_{i-1} to the second equation. It is convenient to let the Laplacian term $k_2(h_{i+1} - 2h_i + h_{i-1})$ appear by defining the variable $u_i = \phi_i - h_i + h_{i-1} - \phi_{i-1}$:

$$\eta \partial_t h_i = f_i^{\text{dis}}(h_i) + k_0(w - h_i) + k_1(h_{i+1} - 2h_i + h_{i-1})$$
$$+ k_2(h_{i+1} - 2h_i + h_{i-1}) - k_2 u_i$$
$$\eta_u \partial_t u_i = k_2(h_{i+1} - 2h_i + h_{i-1}) - k_2 u_i \quad \text{[A3]}$$

To generalize this to higher dimensions (on a square lattice), one simply has to connect each block h_i to its neighbours via symmetrically arranged viscoelastic elements. The equations obtained are exactly the same, with the label i now referring to d-dimensional space, the $d = 1$ discrete Laplacian replaced with the d-dimensional Laplacian denoted Δ, and the u_i variable redefined as:

$$u_i = \sum_{j=1}^{d}(\phi_j - h_j) + \sum_{j'=d+1}^{2d}(h_{j'} - \phi_{j'}) \quad \text{[A4]}$$

In this way, one obtains Eqs. (3), (4) of the main text.

It is worth to notice that the dynamics of the model without relaxation is fully justified by the Middleton theorem [1] which guarantees that the interface moves only forward. However, in presence of viscoelastic elements

---

[1] The graphical representation of the term $\eta \partial_t h_i$ in Eq.[A1] would be a dashpot connecting h_i to the "ground" position $h = 0$.

the Middleton theorem does not apply, and backward movements of the interface are possible. Fortunately, these movements are not frequent, due to the biased driving term $k_0(w-h)$ and we observed numerically that the real dynamics yields the same statistical results as the dynamics that allows only forward movements. Thus, we restrain the dynamics to forward movements.

Appendix B: Mean field analysis

In general, the mean field limit can be studied using models which are much simpler than their finite dimension counterpart. For example, the mean field depinning can be mapped [2] onto the problem of a single particle driven in a Brownian force landscape, the so-called ABBM model [3]. Many results on the avalanche statistics of the mean field interface can be obtained from this latter model [4, 5]. Unfortunately, such a mapping does not hold in presence of relaxation. A different strategy, which can be generalized to that case, is to consider the fully connected model, where each site interacts with all the others.

In the fully connected model, all sites are equivalent and the δ_i's are independent and identically distributed variables, characterized by their probability distribution $P_w(\delta)$ which in general depends on the the initial condition $P_0(\delta)$ and on the value of w. The aim of this section is to write down the evolution equation for $P_w(\delta)$ when w increases. We will show that in the depinning case the distribution reaches a stationary form, while the viscoelastic depinning displays a periodic solution.

1. Reference material for the depinning model

By replacing the local term $(\Delta h)_i$ in Eq.(6) of main text with its fully connected version $\bar{h} - h_i$, we obtain:

$$\delta_i = f^{\text{th}} - k_0(w - h_i) - k_1(\bar{h} - h_i) \qquad [\text{B1}]$$

Let us set the threshold force f^{th} to be constant, a choice that, for the mean field analysis, does not alter the results.

When the external driving is increased by a small positive quantity ẇ, the distribution evolves from its initial shape $P_w(\delta)$, to a new shape $P_{w+\text{ẇ}}(\delta)$. In order to compute the latter, it is useful to decompose the dynamical evolution in different steps. In a first step, the center of the parabolic potential moves from w to $w+\text{ẇ}$, and all δ_i's decrease by $d\delta = k_0\text{ẇ}$, moreover, a fraction $P_w(0)k_0\text{ẇ}$ of sites becomes unstable and moves to the next wells. The new δ_i are given by $z(k_1 + k_0)$, with z's drawn from the distribution $g(z)$. This writes:

$$\frac{P_{\text{step1}}(\delta) - P_w(\delta)}{k_0\text{ẇ}} = \frac{\partial P_w}{\partial \delta}(\delta) + P_w(0)\frac{g\left(\frac{\delta}{k_0+k_1}\right)}{k_0 + k_1} \quad [\text{B2}]$$

The redistribution of δ's changes $\bar{h}$ of a quantity $P_w(0)\bar{z}k_1$, so that all blocks are subject to a shift in their δ_i. This can induce a second step which acts on $P_{\text{step1}}(\delta)$ exactly as step1 did on $P_w(\delta)$, but with a shift $d\delta = P_w(0)\bar{z}k_1$. These steps go on until there are no more unstable sites, so that the distribution reaches the stable form $P_{w+\text{ẇ}}(\delta)$. Let us remark that Eq.[B2] has a fixed point $P_*(\delta)$ found when

$$\frac{\partial P_*}{\partial \delta}(\delta) + P_*(0)\frac{g\left(\frac{\delta}{k_0+k_1}\right)}{k_0 + k_1} = 0. \qquad [\text{B3}]$$

This equation can be easily integrated and $P_*(0)$ determined by the normalization condition. This gives:

$$P_*(\delta) = Q(\delta, k_1) = \frac{1 - G(\frac{\delta}{k_0+k_1})}{\bar{z}(k_0 + k_1)}, \qquad [\text{B4}]$$

where $G(z) \equiv \int_0^z dz' g(z')$. A stability analysis shows that the fixed point is attractive, so that any initial condition converges to it. Moreover, it is possible to prove that for a given initial condition, there exists a finite w_* at which the distribution reaches the fixed point and remains there for $w > w_*$. This indicates that the large time dynamics is stationary, and that the applied stress in the system is constant in time:

$$\bar{\sigma}(k_1) \equiv f^{\text{th}} - \bar{\delta}(k_1). \qquad [\text{B5}]$$

This result becomes $\bar{\sigma}(k_1) = f^{\text{th}} - (k_0 + k_1)\bar{z}$ for an exponentially distributed z.

For the depinning case, we can also compute the probability distribution of the avalanche sizes $N(S)$ in the fully connected approximation, for finite values of the parameters $k_0, k_1, \bar{z}$. Let us first consider the case where $g(z) = \delta(z - \bar{z})$. For a finite system with N sites, the typical configuration $\{\delta_i\}$ corresponds to a set of N independent and identically distributed random variables drawn from $P(\delta)$. Let us sort the set: $\delta_0 < \delta_1 < \cdots < \delta_{N-1}$. When the system becomes unstable we have by definition $\delta_0 = 0$. This site jumps to the next well at distance $\bar{z}$, so that all δ_i's are decreased by $\bar{z}k_1/N$. This will produce at least another jump if $\delta_1 < \bar{z}k_1/N$. More generally, the avalanche size S corresponds to the first time that the relation:

$$\delta_{S-1} \leq \bar{z}k_1\frac{S}{N} < \delta_S \qquad [\text{B6}]$$

is fulfilled.

It is thus important to study the statistics of the δ_i when $i \ll N$. Let us observe that when N is very large the distribution of these δ_i's can be approximated with a uniform distribution: $P(\delta) \sim P(0)$. Within this approximation, the spacings $X_i = \delta_{i+1} - \delta_i$ are independent exponential variables of mean $1/P(0)N$ and variance $1/(P(0)N)^2$. We conclude that the sequence $\delta_0, \ldots, \delta_i$ is a random walk of diffusion constant $1/(P(0)N)^2$ and

drift $1/(P(0)N)$.

The statistics of S thus corresponds to the problem of first crossing with 0 of a random walk with diffusion constant $D = 1/(P(0)N)^2$ and drift $d = \frac{\bar{z}k_1}{N} - \frac{1}{P(0)N}$. For a positive drift, there is a finite probability that this random walk never crosses 0, which corresponds to a *global* event. For a negative drift, the time of zero crossing is always finite, and has been computed for the Brownian motion in [6]. The distribution of the avalanche sizes thus reads:

$$N(S) \sim S^{-3/2} e^{-S/2S_{\max}}$$

$$\text{with } S_{\max} = \frac{D}{d^2} = (1 - P(0)\bar{z}k_1)^{-2} \qquad [\text{B7}]$$

where for simplicity we have neglected the short-scale regularization in the expression of $N(S)$. If now we replace the choice $g(z) = \delta(z - \bar{z})$ with a broader function $g(z)$, the results of Eq.[B7] still hold but with a different diffusion constant. Finally let us remark that the results we obtain here focusing on δ_i, coincide with the results obtained using the mapping to the ABBM model.

2. Mean field analysis of the model with relaxation

The fully connected approximation for the model with viscoelastic elements is obtained by replacing $(\Delta h)_i$ in Eq.[7] by $\bar{h} - h_i$, as for the depinning model:

$$\delta_i = f^{\text{th}} - k_0(w - h_i) - (k_1 + k_2)(\bar{h} - h_i) + k_2 u_i. \quad [\text{B8}]$$

It is useful to split δ in a *fast* part, δ^F, and a *relaxed* one, δ^R:

$$\delta_i^F = f^{\text{th}} - k_0(w - h_i) - (k_1 + k_2)(\bar{h} - h_i)$$
$$\delta_i^R = k_2 u_i. \qquad [\text{B9}]$$

Under a small increase of w, two dynamical regimes are observed. On the short time scales ($t \simeq \tau$) the dashpots are blocked, so that all δ_i^R's remain constant while all δ_i^F are shifted by $k_0 w$. Sites that become unstable (i.e. with $\delta_i = \delta_i^F + \delta_i^R \leq 0$) move to their next pinning well, following the rules of the rigid depinning interface, with stiffness $k_1 + k_2$. On longer time scales ($t \simeq \tau_u$) the dashpots relax, so that δ_i^R's slowly evolve and can possibly trigger new fast events called aftershocks. Within the approximation $f^{\text{th}} = $ cte, no aftershocks are observed. This allows the blocks to fully relax after each event, so that the system's state just before any event is always fully relaxed ($u_i = \bar{h} - h_i$). This corresponds to a relaxed δ_i^R:

$$\delta_{i,\infty}^R = k_2(\bar{h} - h_i) = k_2 \frac{\overline{\delta^F} - \delta_i^F}{k_0 + k_1 + k_2} \qquad [\text{B10}]$$

where the last equality is obtained by inverting Eqs.[B9]. The effect of an event is to modify the distribution of δ^F
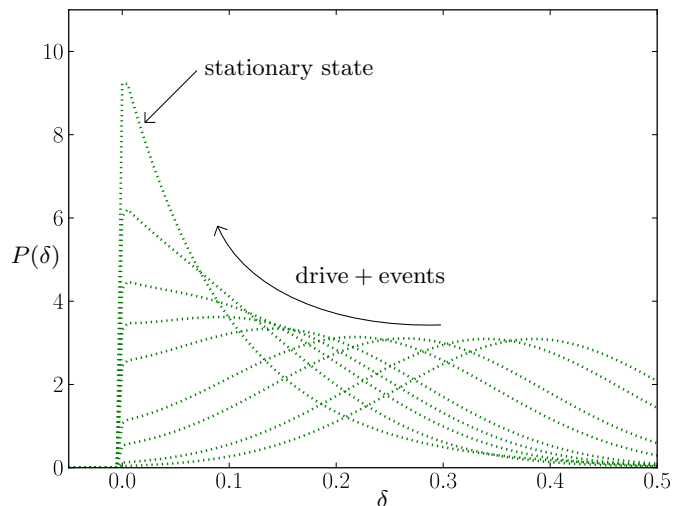

FIG. 7: The evolution of $P_w(\delta)$ for the quenched Edwards-Wilkinson model when w is increased. The initial distribution is a Gaussian centred in $\delta = 0.4$, with standard deviation 0.15, and the weight at the left of $\delta = 0$ cut. $P(\delta)$ quickly reaches its stationary form.

which, just before an event, is related to $P_w(\delta)$ (using Eq.[B10]):

$$\widetilde{P}_w(\delta^F) = \kappa P_w(\kappa(\delta^F + \delta^*)), \qquad [\text{B11}]$$

where $\delta^* = k_2\bar{\delta}/(k_0 + k_1)$ and $\kappa = (k_0 + k_1)/(k_0 + k_1 + k_2)$. At the first step of the event, the unstable sites are those with $\delta^F = -\delta^*$, so that $\widetilde{P}$ evolves from $\widetilde{P}_w$ to $\widetilde{P}_{\text{step1}}$ via:

$$\frac{\widetilde{P}_{\text{step1}} - \widetilde{P}_w}{k_0 w} = \frac{\partial \widetilde{P}_w}{\partial \delta^F} + \frac{\widetilde{P}_w(-\delta^*)}{k_0 + k_1 + k_2} g\left(\frac{\delta^F + \delta^*}{k_0 + k_1 + k_2} \right)$$
$$[\text{B12}]$$

this equation has a depinning-type fixed point $\widetilde{P}_*(\delta^F) = Q(\delta^F + \delta^*, k_1 + k_2)$, which translates for the variable δ in the fixed point $P_*(\delta) = Q(\delta, k_1)$ of the depinning model for the more flexible interface (with stiffness k_1). We conclude that when the dynamics consists in avalanches of very few *steps* (here we assume just one), the distribution $P_w(\delta)$ converges to this attractive fixed point.

This convergence, observed in Fig. 3a of the main text, stops when $P_w(\delta)$ overcomes the fixed point of the rigid interface at $\delta = 0$, namely $P_w(0) \geq (\bar{z}(k_1 + k_2))^{-1}$. At this stage, a global avalanche is triggered in the system[2], and $P_w(\delta)$ jumps to the fixed point $Q(\delta, k_1 + k_2)$ of the rigid interface (stage 3). Finally, at the end of this

---

[2] For avalanches that last for more than one step, the evolution of $P_w(\delta)$ can not be computed from Eq.[B12] because the system is not fully relaxed during the avalanche. Instead it is necessary to follow the evolution of the joint probability distribution $P(\delta^F, \delta^R)$. The details of this numerical integration are given in the SI Text Sec. 4+1

global event, relaxation takes the system far from this fixed point, and a new cycle starts (stage 4).

Appendix C: Fully connected model: numerical integration of the evolution equations of $P(\delta)$

1. Numerical integration for the depinning model

Let us discretize $P(\delta)$ with a bin of size ε. The distribution probability is then a vector P_i (related to $P(\delta)$ by $P_i = P(\delta = \varepsilon i)$) which evolves with the following rules:

- *Driving process*: We shift P_i of one bin: $P_i \leftarrow P_{i+1}$.

- *Instability check*: We compute the weight of unstable sites:

$$P_{\text{inst}} = \varepsilon \sum_{i<0} P_i$$

If $P_{\text{inst}} > 0$, we perform the *Avalanche process*. Else we go back to the *Driving process*.

- *Avalanche process*: it is composed by a stress drop and a stress shift.

  – Stress drop:

  $$P_{i\geq0} \leftarrow P_i + P_{\text{inst}} \frac{g\left(\varepsilon i/(k_0 + k_1)\right)}{k_0 + k_1}$$
  $$P_{i<0} \leftarrow 0$$

  – Stress shift: we shift P_i of $n_{\text{shift}} = \text{Int}\left[\frac{\bar{z}k_1 P_{\text{inst}}}{\varepsilon}\right]$ bins.

  $$P_i \leftarrow P_{i+n_{\text{shift}}}$$

Then we perform the *Instability check*.

This algorithm converges very quickly from any initial configuration to $P_*(\delta)$ for any choice of $g(z)$, see Fig. 7 of the SI Text.

2. Numerical integration for the model with relaxation

Analogously to the previous case, we discretize $P(\delta^F, \delta^R)$ with a bin ε. The distribution probability is then a matrix $P_{i,j}$ where $P_{i,j} = P(\delta^F = \varepsilon i, \delta^R = \varepsilon j)$. The matrix evolves with the following rules:

- *Driving process*: We shift $P_{i,j}$ of one bin: $P_{i,j} \leftarrow P_{i+1,j}$.

- *Instability check*: We compute the weight of unstable sites:

$$P_{\text{inst}} = \varepsilon \sum_{(i+j)<0} P_{i,j}$$

If $P_{\text{inst}} > 0$, we perform the *Avalanche process*. Else we perform the *Relaxation process*

- *Avalanche process*: it is composed by a stress drop and a stress shift.

  – Stress drop: $\forall(i,j)$,

if $i + j \geq 0$:

$$P_{i,j} \leftarrow P_{i,j} + \frac{\varepsilon}{\kappa} \left(\sum_{i' | (i'+j<0)} P_{i',j} \right) g\left(\frac{\varepsilon(i+j)}{\kappa} \right),$$

if $i + j < 0$:

$$P_{i,j} \leftarrow 0,$$

  where $\kappa = k_0 + k_1 + k_2$.
  – Stress shift: we shift $P_{i,j}$ of
  $n_{\text{shift}} = \text{Int}\left[\frac{\bar{z}(k_1+k_2)P_{\text{inst}}}{\varepsilon}\right]$ bins.

  $$P_{i,j} \leftarrow P_{i+n_{\text{shift}},j}$$

Then we perform the *Instability check*.

- *Relaxation process*: We compute, $j_\infty(i)$, the single bin associated to $\delta_{i,\infty}^R = j_\infty(i)\varepsilon$ as[3]

$$j_\infty(i) = \text{Int}\left(k_2 \frac{-i + \sum_{i',j} i' P(i',j)}{\kappa} \right)$$

so that the relaxation corresponds to:

$$P_{i,j_\infty(i)} \leftarrow \sum_j P_{i,j}$$
$$P_{i,j\neq j_\infty(i)} \leftarrow 0$$

Then we perform the *driving process*.

This algorithm integrates the fully connected version of the viscoelastic model, and produces the results shown in Fig. 3 of the main text.

Appendix D: Two dimensional case: details on the numerical integration procedure

We provide here details on the integration of the dynamic equations of the viscoelastic model. Our starting point are the equations (3) and (4) of the main text:

$$\eta \partial_t h_i = k_0(w - h_i) + f_i^{\text{dis}}(h_i) + k_1 \Delta h_i + k_2(\Delta h_i - u_i) \tag{D1}$$

$$\eta_u \partial_t u_i = k_2(\Delta h_i - u_i) \tag{D2}$$

———————

[3] It is numerically more stable to associate $\delta^R(i,\infty)$ with two bins, $j_\infty(i)$ and $j_\infty(i) + 1$. The contribution $\sum_j P_{i,j}$ is splitted in the two bins using a linear interpolation.

with $w = V_0 t$. For the numerical work, it is convenient to introduce variables F_i and G_i, defined as

$$F_i \equiv k_2(\Delta h_i - u_i) \qquad \text{[D3]}$$
$$G_i \equiv k_1(\Delta h_i) + k_0(w - h_i) \qquad \text{[D4]}$$

Using F_i and G_i, the model equations can be written as

$$\eta \partial_t h_i = f_i^{\text{dis}}(h_i) + G_i + F_i \qquad \text{[D5]}$$
$$\eta_u \partial_t F_i + k_2 F_i = \eta_u k_2 (\Delta \partial_t h)_i. \qquad \text{[D6]}$$

It is thus clear that G_i represents the force onto h_i exerted through k_1 and k_0 springs, whereas F_i is the force coming from the branches that contain the dashpots and k_2 springs.

We work in the case in which temporal scales are well separated: $\tau \ll \tau_u \ll \tau_D$. This corresponds to $\eta \ll \eta_u \ll \bar{z} k_0 / V_0$. As discussed in the main text, within the narrow well approximation the actual integration of Eqs. [D5] and [D6] does not need a continuous time algorithm, but can be presented in the form of a discrete set of rules. From a relaxed configuration with $F_i = 0$ at time t, the load increase triggers a new instability of Eq.[D5] when f_i^{dis} (which is negative) reaches $-f_i^{th}$, and this occurs after a time interval:

$$\delta t = \min_i \left(\frac{f_i^{th} - G_i}{k_0 V_0} \right) \qquad \text{[D7]}$$

Thus at time $t + \delta t$ an avalanche starts at position i, producing the advance of h_i to the next potential well $h_i \leftarrow h_i + z$, and a corresponding rearrangement of the forces according to (in two dimensions):

$$F_i \leftarrow F_i - 4k_2 z \qquad \text{[D8]}$$
$$G_i \leftarrow G_i - (4k_1 + k_0)z \qquad \text{[D9]}$$
$$F_j \leftarrow F_j + k_2 z \qquad \text{[D10]}$$
$$G_j \leftarrow G_j + k_1 z \qquad \text{[D11]}$$

where j are the four neighbour sites to i, and the value of f_i^{th} is renewed from its probability distribution. All successive unstable sites are treated in the same way until there are no more unstable sites. This defines the primary avalanche. At this point the relaxation dynamics [D6] begins to act, until some site eventually becomes unstable. Note that due to the discrete pinning potential, in this stage h remains constant, namely the relaxation dynamics is simply:

$$\eta_u \partial_t F_i = -k_2 F_i, \qquad \text{[D12]}$$

This means that a given site i will trigger an avalanche due to relaxation if for some increase in time δt the pin-

ning force f_i^{dis} on this site reaches $-f_i^{th}$, i.e., if

$$F_i e^{\frac{-k_2 \delta t}{\eta_u}} + G_i = f_i^{th}, \qquad \text{[D13]}$$

(note that in order to have a solution, F_i must be negative, as the l.h.s is lower that the r.h.s. at the starting time). This leads to the determination of δt as

$$\delta t = -\frac{\eta_u}{k_2} \min_i \left[\ln \left(\frac{f_i^{th} - G_i}{F_i} \right) \right] \qquad \text{[D14]}$$

Once all the secondary avalanches generated by relaxation have been produced and F_i has relaxed to zero, the external driving is increased again, according to [D7].

This is the main scheme of the simulation. We should mention however, that its efficient implementation relies on a classification scheme of all sites, in such a way that the determination of the next unstable site in [D7] and [D14] does not require a time consuming sweep over the whole lattice. In fact, following Grassberger[7] we classify the sites according to their value of the r.h.s. of [D7] and [D14], and bin them, in such a way that the determination of the next unstable site can be limited to the bin corresponding to the lowest values of these quantities. When sites change their h values along the simulation, they are reaccomodated in the bins using a linked list algorithm.

Appendix E: Methods

For Figs. 1, 2, 4, 5 and 6, the numerical method used is the one described in SI Section 3. In Figs 1 and 2, the number of blocks is $512^2 = 65536$ (in 2D, we consider a square-shaped interface with $L = 512$). We use $k_0 = 0.02, k_1 = 0.5, g(z) = e^{-z}$ and the thresholds f_i^{th} are distributed as a Gaussian of mean 3 and unit variance. In Fig. 1 we use $k_2 = 0$, i.e. we simulate the conventional depinning model. In Fig. 2 we use $k_2 = 0.5$, and the grey lines represent the stress averaged in small patches of size 10×10 (100 blocks). The two patches are chosen to be as far as possible.

In Fig. 3 we perform the simulation described in SI Section 5 (and in particular in Sec. 5.2). We use $k_0 = 0.001, k_1 = 0.1, k_2 = 0.3, g(z) = e^{-z}$ and the thresholds are set constant $f_i^{\text{th}} = 1, \forall i$. The discretization of δ^F and δ^C is made using a binning $\varepsilon = 0.003$.

In Fig. 4, 5 and 6, we use $k_1 = 0, k_2 = 1$. $g(z)$ is the uniform distribution in the range $[0, 0.2]$. The f_i^{th} are distributed as in Figs. 1 & 2. The number of blocks is $15000^2 = 225000000$ (with $L = 15000$). In Fig. 5 we used $k_0 = 0.012$.

[1] Middleton, A. A. Asymptotic uniqueness of the sliding state for charge-density waves. *Physical review letters* **68**, 670–673 (1992).

[2] Zapperi, S., Cizeau, P., Durin, G. & Stanley, H. Dynamics

of a ferromagnetic domain wall: Avalanches, depinning transition, and the Barkhausen effect. *Physical Review B* **58**, 6353–6366 (1998).

[3] Alessandro, B., Beatrice, C., Bertotti, G. & Montorsi, A. Domain-wall dynamics and Barkhausen effect in metallic ferromagnetic materials. I. Theory. *Journal of Applied Physics* **68**, 2901–2907 (1990).

[4] Le Doussal, P. & Wiese, K. Driven particle in a random landscape: Disorder correlator, avalanche distribution, and extreme value statistics of records. *Physical Review E* **79**, 051105 (2009).

[5] Dobrinevski, A., Le Doussal, P. & Wiese, K. J. Non-stationary dynamics of the Alessandro-Beatrice-Bertotti-Montorsi model. *Physical Review E* **85**, 031105 (2012). 1112.6307.

[6] Majumdar, S. & Comtet, A. Exact asymptotic results for persistence in the Sinai model with arbitrary drift. *Physical Review E* **66**, 061105 (2002).

[7] Grassberger, P. Efficient large-scale simulations of a uniformly driven system. *Physical Review E* **49**, 2436–2444 (1994).